"Ship in bottle" Porph@MOMs as highly efficient catalysts for selective controllable oxidation and insights into different mechanism in heterogeneous and homogeneous environment

M. Saghian,[a] S. Dehghanpour*[a] and M. Sharbatdaran[b]

Submitted to the New Journal of Chemistry

Supporting information:

Materials and instrumentation

All reagents were purchased from Sigma-Aldrich and Merck chemical companies and used without further purification. Chemical analyses were performed with Varian 150AX inductively coupled plasma optical emission spectrometer (ICP-OES). Elemental analyses were performed on a Heraeus CHN-O-Rapid elemental analyzer. FT-IR spectra were recorded on a Bruker Tensor 27 FT-IR spectrometer using KBr pellets over the range of 4000–400 cm^{-1}. The X-ray powder diffraction (XRD) data were recorded on a Siefert XRD 3003 PTS diffractometer, using Cu $K_{\alpha 1}$ radiation (k = 1.5406 Å). UV-Vis spectra were obtained with a shimadzu UV-260 spectrophotometer. Scanning electron microscopy (SEM) images were obtained on a Philips XL-30ESEM equipped with an X-ray energy dispersive detector. X-ray photoelectron spectroscopy (XPS) measurements were carried out with a Thermo Scientifi, ESCALAB 250Xi using an Mg X-ray source. The ^{1}H NMR spectra were recorded on a Bruker 400 MHz spectrometer in CD_3COCD_3 solvent. The thermogravimetric analysis (TGA) was performed using a Mettler Toledo TGA/DSC instrument at a heating rate of 10 $^oCmin^{-1}$ in air atmosphere. Oxidation products were analyzed by GC and GC-Mass using Agilent 6890 series with a FID detector, HP-5, 5% phenylmethylsiloxane capillary and Agilent 5973 network, mass selective detector, HP-5 MS 6989 network GC system, respectively**.** Nitrogen sorption isotherms were recorded on a Belsorp Mini–II instrument at 77K.

Synthesis of catalysts

Synthesis and purification of 5, 10, 15, 20- Tetra(4-pyridyl) porphyrin (H_2TPyP). H_2TPyP was synthesized according to the previously reported method [1]. According to the synthesis method, 4-pyridinecarboxaldehyde (1.9 ml, 20 mmol) and fresh distilled pyrrole (1.4 ml, 20 mmol) were added to a mixture of 40 ml of boiling propionic acid and 1 ml of glacial acetic acid. The reaction mixture was refluxed for one hour. The solvent was evaporated under vacuum and the oily residue was washed with hot water, diluted with ammonia solution (25%) and washed with hot water again. The slightly wet material was stirred with methanol on a steam bath and placed in a freezer overnight. The purple solid was filtered off and passed through a silica gel column chromatography using a mixture of methanol and dichloromethane as the eluent, for further purification. UV-Vis (DMF, λ_{max}, nm): 415, 513, 547,587, 643. FT-IR (cm^{-1}, KBr): 3440 (m), 3091 (w), 2923 (w), 1589 (s), 1545 (w), 1464 (w), 1387 (m), 1343 (w), 1215 (w), 968 (m), 793 (s), 721 (m), 659 (m). ^{1}H NMR (ppm): -2.99 (s, 2H, NH), 8.17-8.19 (d, 8H, m), 8.89 (s, 8H, β), 9.08-9.09 (d, 8H, o).

Synthesis and purification of meso-Tetra(N-methyl-4-pyridyl)porphyrin (H_2TMPyP). H_2TMPyP was synthesized according to the previously reported method[2]. For synthesis, H_2TPyP (200 mg, 0.33 mmol) was dissolved in 30 ml of N, N-dimethylformamide and 9 ml of methyl iodide was added to the mentioned solution. The solution thus obtained was stirred for 10 hours at room temperature. After evaporating the solvent under vacuum at room temperature, the resulting powder was recrystallized in a mixture of methanol and ethyl acetate. UV-Vis (H_2O, λ_{max}, nm): 424, 519, 557, 586, 644. FT-IR (KBr, cm^{-1}): 3454 (m), 3035 (w), 1639 (s), 1566 (m), 1521 (w), 1463 (m), 1398 (w), 1244 (s), 1066 (w), 997 (m), 802 (m), 734 (m). ^{1}H NMR (ppm): -3.11 (s, 2H, NH), 4.73 (s, 12H, N─CH3), 8.99-9.01 (d, 8H, m), 9.20 (s, 8H, β), 9.48-9.50 (d, 8H, o).

Synthesis of Iron tetra(N-methyl-4-pyridyl)porphyrin (FeTMPyP). FeTMPyP was synthesized according to the previously reported method[3]. In accordance with the synthesis method, H_2TMPyP (200 mg, 0.17 mmol) was dissolved in water and the excess amount of iron chloride tetrahydrate (270 mg, 1.36 mmol) was added to the solution. The obtained solution was refluxed for two hours. After confirming the formation of the desired complex, the reaction mixture was cooled and the intended metalloporphyrin was precipitated by adding excess amount of sodium

perchlorate. UV-Vis (H_2O, λ_{max}, nm): 421, 597, 637. FT-IR (KBr, cm^{-1}): 3033(w), 1635(s), 1519(w), 1454(m), 1336(w), 1274(w), 1186(w), 1083(w), 997(m), 802(m), 717(w), 522(w).

Synthesis of Cobalt tetra(N-methyl-4-pyridyl)porphyrin (CoTMPyP). Preparation of CoTMPyP was carried out by using the previously reported method[4]. In atypical synthesis, excess $CoCl_2.6H_2O$ (243 mg, 1.02 mmol) was added to a solution containing H_2TMPyP (200 mg, 0.17 mmol) in water and the resulting mixture was refluxed overnight. Afterwards, the solution was cooled and excess sodium perchlorate was added to the reaction mixture in order to precipitate metalloporphyrin. UV-Vis (H_2O, λ_{max}, nm): 436, 550, 655. FT-IR (KBr, cm^{-1}): 3030(w), 1632(s), 1511(w), 1454(m), 1332(w), 1273(w), 1185(w), 1081(w), 996(m), 798(m), 711(w), 520(w).

Synthesis of manganese tetra(N-methyl-4-pyridyl)porphyrin (MnTMPyP). MnTMPyP was prepared by using the previously reported method[5]. In this way, first MnTPyP was synthesized according to the following procedure. Manganese acetate (502 mg, 2.9 mmol) and H_2TPyP (200 mg, 0.33 mmol) were mixed in glacial acetic acid (100 ml) and the resulting mixture was refluxed for 6 hours. The solution obtained was cooled and solvent was evaporated under vacuum. The solid residue was dissolved in hot water and a precipitate formed by adding sodium acetate. The prepared solid was filtered off and washed with cold water. MnTMPyP was synthesized by addition of methyl iodide (25 ml) to MnTPyP (0.5 g, 0.74 mmol). The reaction mixture was stirred for two days at room temperature, followed by filtration and drying under vacuum. UV-Vis (H_2O, λ_{max}, nm): 462, 569, 674. FT-IR (KBr, cm^{-1}): 3034(w), 1636(s) , 1521(w), 1455(m), 1336(w), 1272(w), 1188(w), 1085(w), 997(m), 805(m), 719(w), 526(w).

Synthesis of Fe-BTC framework. Preparation of Fe-BTC was carried out by using the previously reported method[6]. In this way, two solutions were prepared for synthesis. (1) NaOH (150 mg, 3.7 mmol) was dissolved in 10 ml of water and trimesic acid (263 mg, 2.25 mmol) was then added to the solution. (2) $FeCl_3.6H_2O$ (508 mg, 2.41 mmol) was added to 10 ml of water to form a yellowish orange solution. Solution 2 was added slowly to the colorless solution 1 and the mixture thus obtained was stirred at room temperature for 6 h. The resulting solid powder was separated by centrifugation and washed with deionized water and ethanol, respectively. FT-IR (KBr, cm^{-1}): 3435(m), 1627(s), 1567 (m), 1450(m), 1381(s), 1113(w), 941(w), 760(m), 712(m), 621(w), 473(w).

Synthesis of Co-BTC framework. Co-BTC was synthesized according to the previously reported method[7]. In atypical procedure, cobalt (II) nitrate hexahydrate (515 mg, 1 mmol), trimesic acid (105 mg, 1 mmol), N,N-dimethylformamide (15 ml) and glacial acetic acid (5 ml) were mixed at room temperature. The resulting solution was transferred to a 25 ml Teflon-lined steel autoclave and heated at 170 °C for 2 days. The purple solid was filtered and washed with dimethylformamide and glacial acetic acid. FT-IR (KBr, cm^{-1}): 3443(m), 2881(m), 1626(s), 1566(m), 1439(m), 1380(s), 1335(m), 1101(m), 943(w), 775(m), 713(m), 671(m), 564(w), 469(w). Anal. Calc. for $C_7H_9CoNO_5$ (M= 246.08 $g.mol^{-1}$): C, 34.13; H, 5.68; N, 3.65. Found: C, 34.05; H, 5.66; N, 3.61.

Synthesis of Mn-BTC framework. Mn-BTC was prepared using the previously reported method[8]. In atypical synthesis, $MnCl_2.4H_2O$ (198 mg, 1.0 mmol), Trimesic acid (210 mg, 1.0 mmol), N, N-dimethylformaide (8 ml), H_2O (1 ml) and EtOH (1 ml) were mixed and the resulting mixture was then stirred at room temperature. The solution was placed in a 25 ml Teflon-lined steel autoclave and heated at 70 °C for 2 days after which it was cooled slowly to room temperature. The light yellow crystals were separated by centrifugation and washed with aforementioned solvents. FT-IR (KBr, cm^{-1}): 3443(m), 2928(m), 1638(s), 1565(m), 1433(m), 1374(s), 1102(m), 937(m), 768(m), 709(m), 672(m), 543(m), 456(m). Anal. Calc. for $C_7H_9MnNO_5$ (M= 242.09 $g.mol^{-1}$): C, 34.69; H, 5.78; N, 3.71. Found: C, 34.60; H, 5.75; N, 3.67.

Synthesis and purification of Porh@MOM-5. Porph@MOM-5 was prepared according to the previously reported method[9]. Typically, $CoCl_2.6H_2O$ (238 mg, 1.0 mmol), Trimesic acid (105 mg, 0.5 mmol), and H_2TMPyP (14 mg, 0.0105 mmol), N, N-dimethylformaid (15 ml), H_2O (2.5 ml) were mixed and homogenized by stirring at room temperature. The resulting dark red solution was transferred to Teflon-lined steel autoclave and heated at 85 °C for 12 h. The resulting solid powder was decanted and washed with methanol. FT-IR (KBr, cm^{-1}): 3377 (m), 1623 (s), 1571 (m), 1440 (m), 1375 (s), 1114 (w), 1014 (w), 948 (w), 763 (m), 721 (m), 574 (w).

Synthesis and purification of Porh@MOM-6. Porph@MOM-6 was prepared according to the previously reported method[9]. For synthesis, a similar procedure as that for Porph@MOM-5 synthesis was used, except for using $MnCl_2.4H_2O$ (192 mg, 1.0 mmol)

instead of $CoCl_2.4H_2O$. FT-IR (KBr, cm^{-1}): 3408 (m), 1629 (s), 1560 (s), 1440 (s), 1373 (s), 1112 (m), 1022 (m), 950 (w), 877 (w), 771 (m), 721 (m), 557 (w).

Characterization of Porphyrins

The UV-Vis spectra of H_2TPyP shows a very sharp intense band (Soret band) in λ=415 nm and four weak absorption bands (Q bands) in the visible region between 500 to 700 nm which are related to π-π* transition of ligand. After methylation of the aforementioned compound to form H_2TMPyP, a small red shift is observed. Therefore, the soret band shifts from 415 to 424 nm (Fig. S21a). Incorporation of different metal ions to free porphyrins causes a red or blue shift in the soret band based on the coordinated metal ion and transformation of four Q-bands to two Q-bands is due to the symmetry changes after metal ion interpolation and formation of metalloporphyrin.[10] Subsequently, iron metalloporphyrin shows a very small blue shift from λ=424 to 421 nm and is identified through the reduction of Q-bands from four to two. Cobalt and manganese metalloporphyrins show red shift from λ=424 nm to λ= 436 and 462 nm, respectively, in addition to the disappearance of Q-bands (Fig. S21b).

^1H NMR analysis was performed to determine the purity of the synthesized compounds. ^1H NMR spectra of H_2TPyP and H_2TMPyP are shown in Fig. S22 and S23, respectively. The results of ^1H NMR reveal that in the free base meso-Tetra(N-methyl-4-pyridyl)porphyrin (Fig. S23), the NH protons appear in -3.11 ppm (singlet), the N-methyl protons become manifest in 4.73 ppm (singlet), the β-pyrrole protons emerge in 9.20 ppm (singlet) and the aryl ring protons exhibit two doublets in the range of 8.99-9.50 ppm, the signals in 8.99-9.01 and 9.48-9.50 ppm are related to meta and ortho hydrogens of aryl ring, respectively.

FT-IR spectra of H_2TPyP is shown in Fig. S24. The FT-IR spectra of H_2TMPyP, FeTMPyP and Porph@MOM-4 are shown in Fig. S1a-c. The FT-IR spectrum of H_2TMPyP (Fig. S1a) displays characteristic bands of porphyrin units at 734 and 802 cm^{-1} which are attributed to the out-of-plane N—H bending vibration and the out-of-plane vibration of C—H in porphyrin ring, respectively. The other N—H bending vibration is observed at 1566 cm^{-1}. The bands appearing at 1200-1600 cm^{-1}, are assigned to the stretching vibrations of C=N and C=C porphyrin ring. Moreover, the stretching vibrations of C—N and C—H pyridyl ring appear at 1639 and 3035 cm^{-1}, respectively. The broad band emerged in 3454 cm^{-1} is related to the N—H pyrrole stretching vibration.[11, 12] Metalation of H_2TPyP compound causes the disappearance of N—H vibration bands due to the metal insertion into the porphyrin periphery. Therefore, disappearing of the bands at 734, 1566 and 3454 cm^{-1} affirms the formation of the corresponding metalloporphyrin which is FeTMPyP (Fig. S1b). Similarly, identical results were obtained for CoTMPyP and MnTMPyP due to the similarity of the structures (Fig. S25 and S26, respectively).

Characterization of Porph@MOMs

In order to investigate the thermal behavior of the synthesized structures, TGA-DSC analysis was carried out. As shown in Fig. S27a, b and c, the weight loss takes place in two or three steps for Porph@MOM-4, Porph@MOM-5 and Porph@MOM-6. The TGA curve of Porph@MOM-4 shows an initial weight loss of 11% between 31-156 °C attributed to the removal of solvent molecules from the lattice. This is accompanied by endothermic peaks in the DSC curve. The sample also showed about 59% weight loss in the 370 °C temperature range, along with exothermic peaks in the DSC curve. The weight loss in this temperature range was primarily associated with decomposition of the MOF (Fig. S27a). Similarly, there was 12% weight loss between 25-235 °C for Porph@MOM-5, along with an endothermic peak in the DSC curve, as the result of the removal of solvent molecules from the framework. The framework decomposition occurred at 420 °C with weight loss of about 57%, along with an exothermic peak in the DSC curve (Fig. S27b). The TGA curve of Porph@MOM-6 showed 15% weight loss between 30-280 °C. This is accompanied by exothermic peaks in the DSC curve corresponding to the loss of solvent molecules within the cavities. Degradation of the structure occurred with a weight loss of about 49% at 460 °C along with an exothermic peak in the DSC curve (Fig. S27c). The residue weights of 30.3, 31.1 and 36.2% could be assigned to the formation of respective metal oxides and are attributed to Fe_3O_4, CoO and MnO_2 for Porph@MOM-4, Porph@MOM-5 and Porph@MOM-6, respectively (calc.: 30.6%, calc.: 31.3% and calc.: 36.4%). The small exothermic peak at 760 °C in three DSC curves without any weight loss is associated with the formation of the crystalline phase of the corresponding metal oxide. Based on these results, the synthesized structures showed high thermal stability.

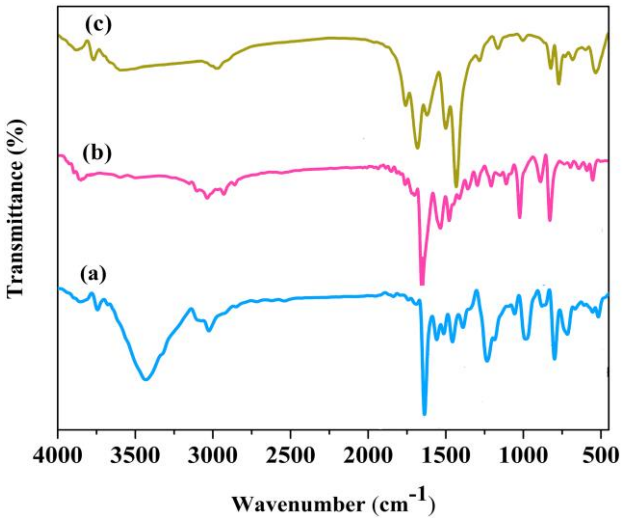

Fig. S1 FT-IR spectra of (a) H_2TMPyP, (b) FeTMPyP and (c) Porph@MOM-4.

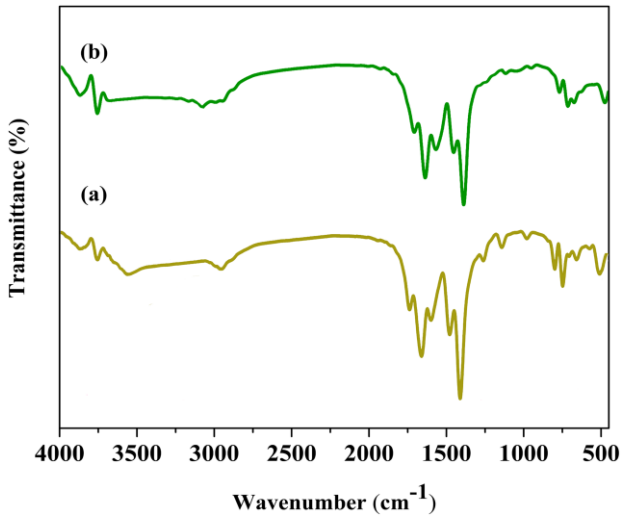

Fig. S2 FT-IR spectra of Porph@MOM-4 (a) before and (b) after using as catalyst.

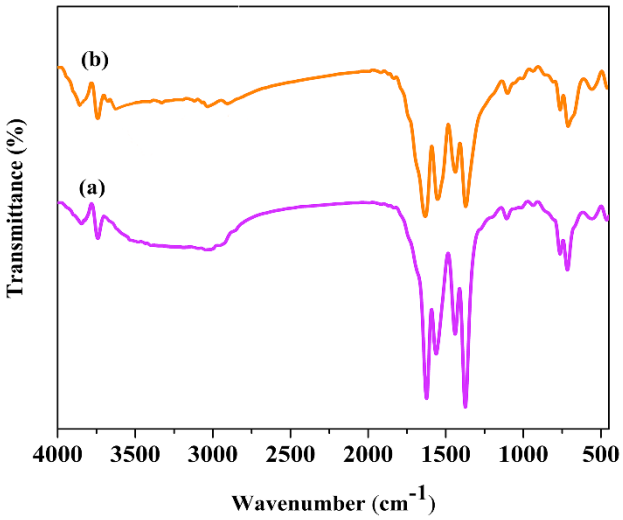

Fig. S3 FT-IR spectra of Porph@MOM-5 (a) before and (b) after using as catalyst.

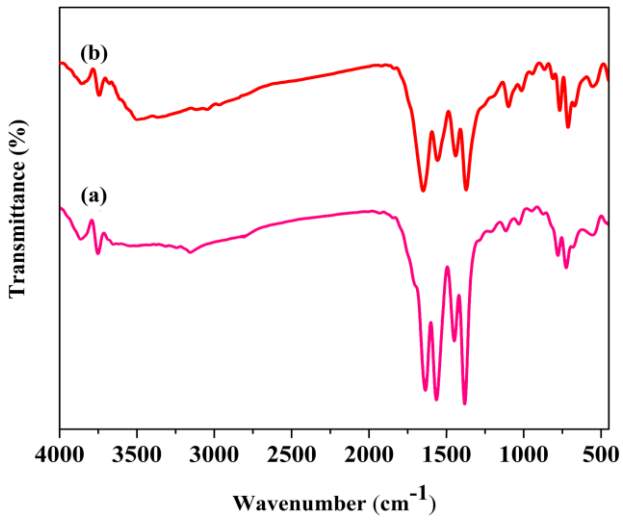

Fig. S4 FT-IR spectra of Porph@MOM-6 (a) before and (b) after using as catalyst.

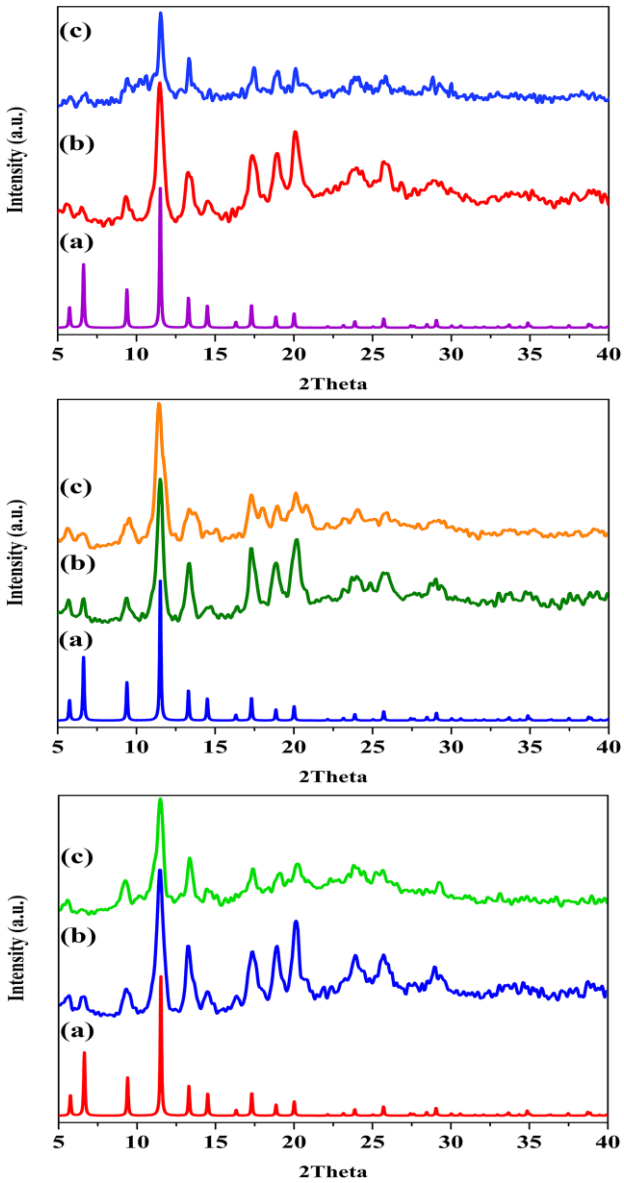

Fig. S5 XRD patterns of Porph@MOM-4 (top), Porph@MOM-5 (middle), and Porph@MOM-6 (bottom), (a) simulated, (b) as-synthesized and (c) recycled samples (after 5 cycles).

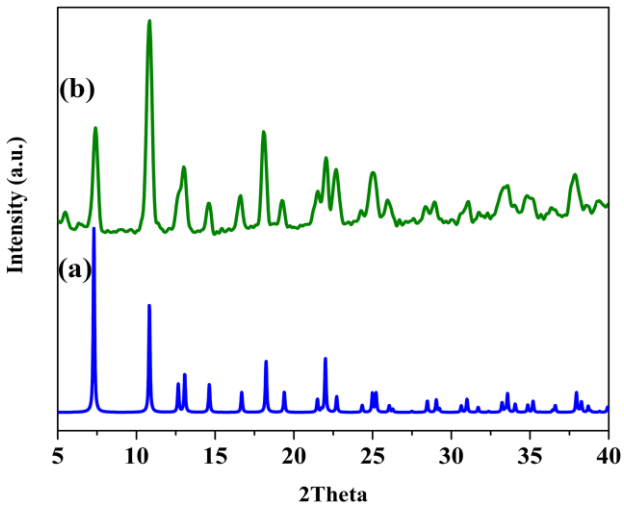

Fig. S6 XRD patterns of CoBTC framework (a) Simulated and (b) as-synthesized.

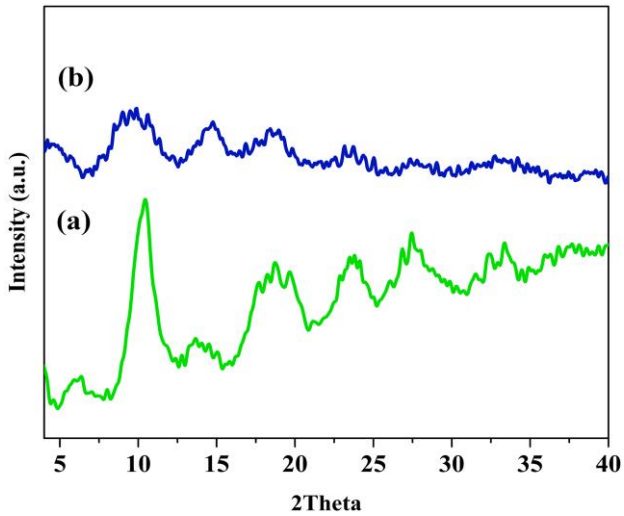

Fig. S7 XRD patterns of FeBTC framework (a) Simulated and (b) as-synthesized.

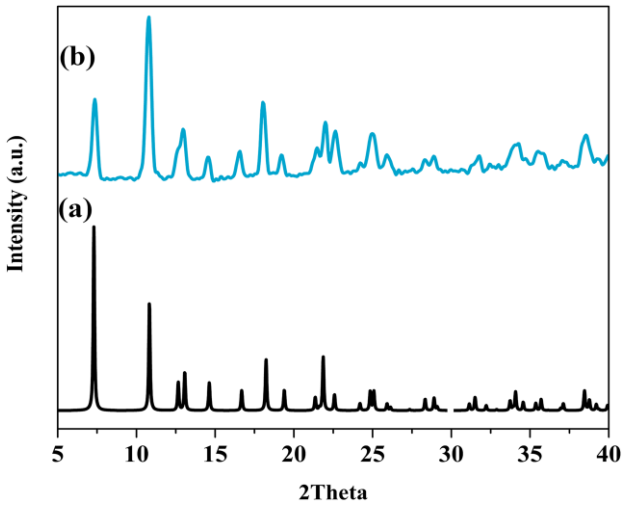

Fig. S8 XRD patterns of MnBTC framework (a) Simulated and (b) as-synthesized.

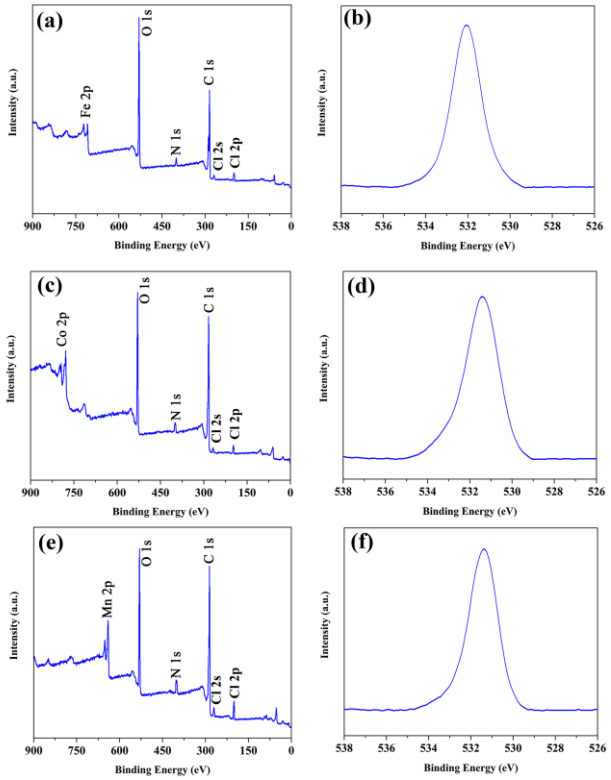

Fig. S9 XPS spectra of Porph@MOM-4 (a) survey spectrum, (b) O 1s, Porph@MOM-5 (c) survey spectrum, (d) O 1s, Porph@MOM-6 (e) survey spectrum, (f) O 1s.

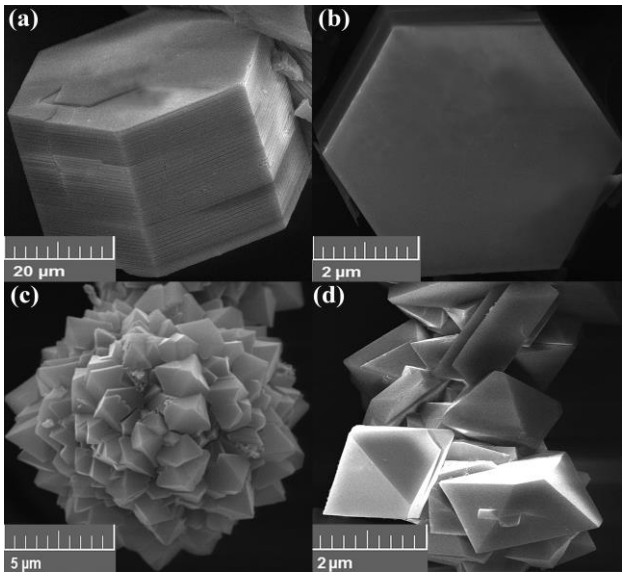

Fig. S10 SEM images of a, b) Cobalt BTC framework and c, d) Porph@MOM-5.

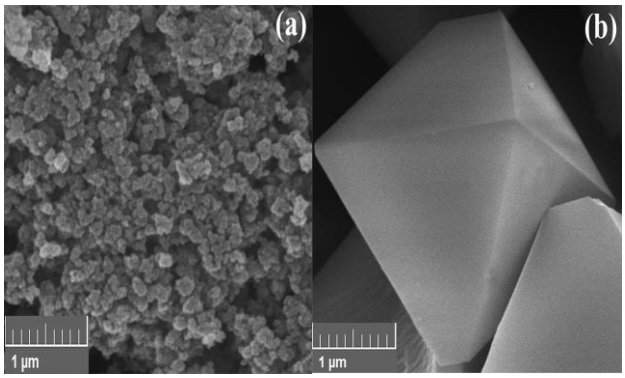

Fig. S11 SEM images of a) Iron BTC framework and b) Porph@MOM-4.

Table S1 N_2 sorption properties of CoBTC and CoTMPyP.

Entry	Sample	S_{BET} ($m^2.g^{-1}$)	Pore volume ($cm^3.g^{-1}$)	Pore diameter (nm)
1	CoBTC	759.15	0.3807	2.0059
2	CoTMPyP	573.25	0.2902	1.7699

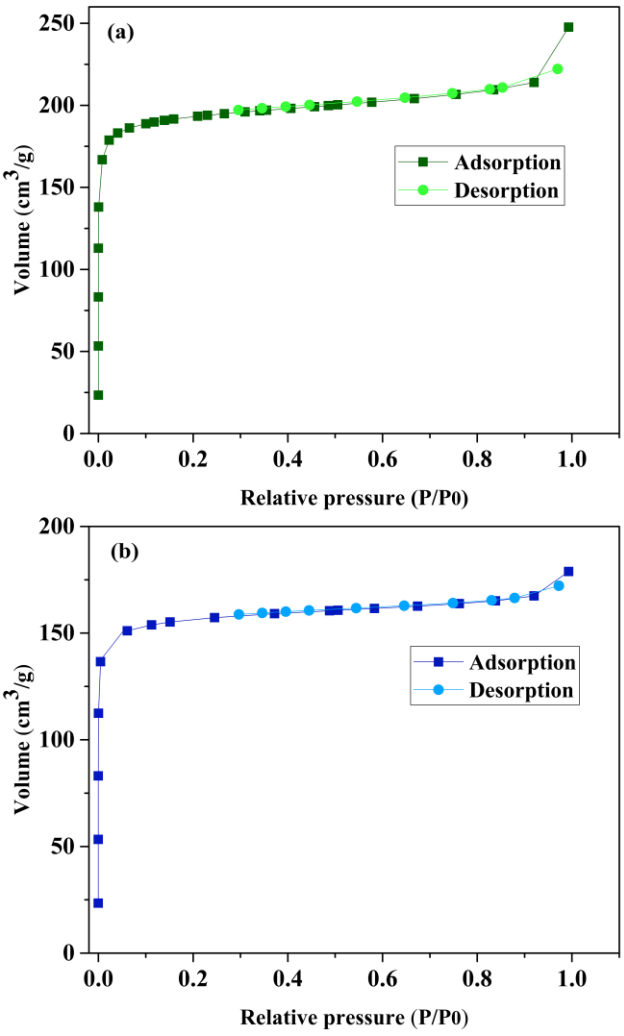

Fig. S12 N_2 adsorption-desorption isotherms of (a) CoBTC and (b) Porph@MOM-5.

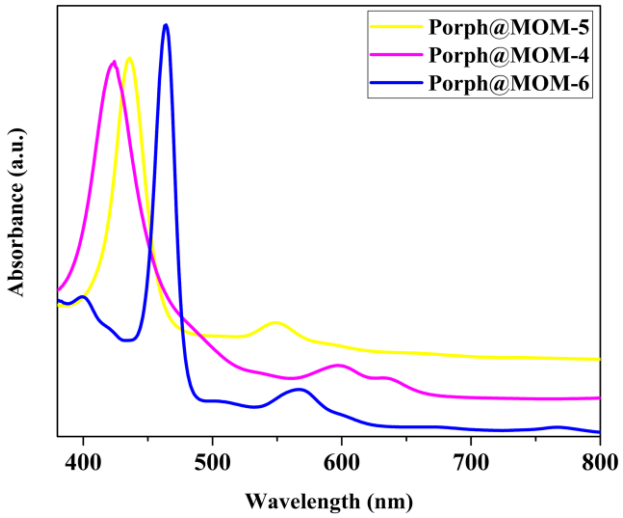

Fig. S13 UV-Vis spectra of Porph@MOM-4 (5.15 mg L^{-1}; purple), Porph@MOM-5 (2.30 mg L^{-1}; yellow) and Porph@MOM-6 (1.10 mg L^{-1}; blue) in water.

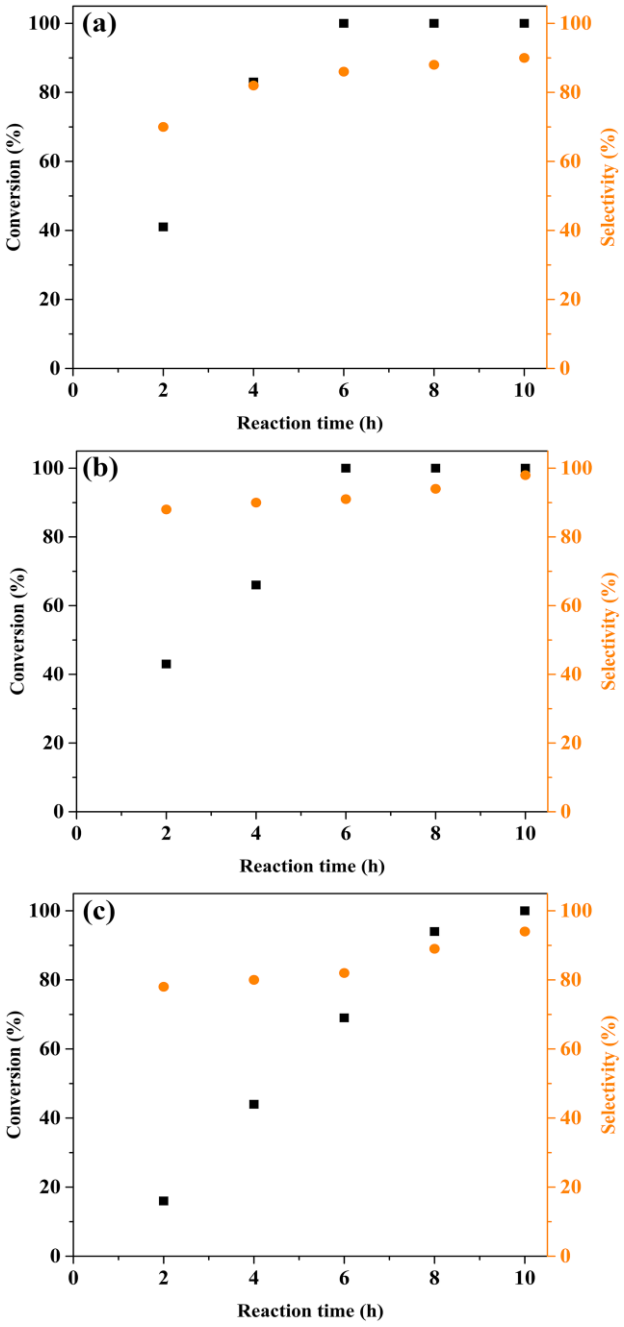

Fig. S14 Kinetic oxidation profiles of cyclohexene with TBHP over (a) catalyst **1** , (b) catalyst **2** and (c) catalyst **3**. Reaction conditions: solvent: acetonitril, cyclohexene (2 mmol), catalyst (5 mg), TBHP (3 mmol).

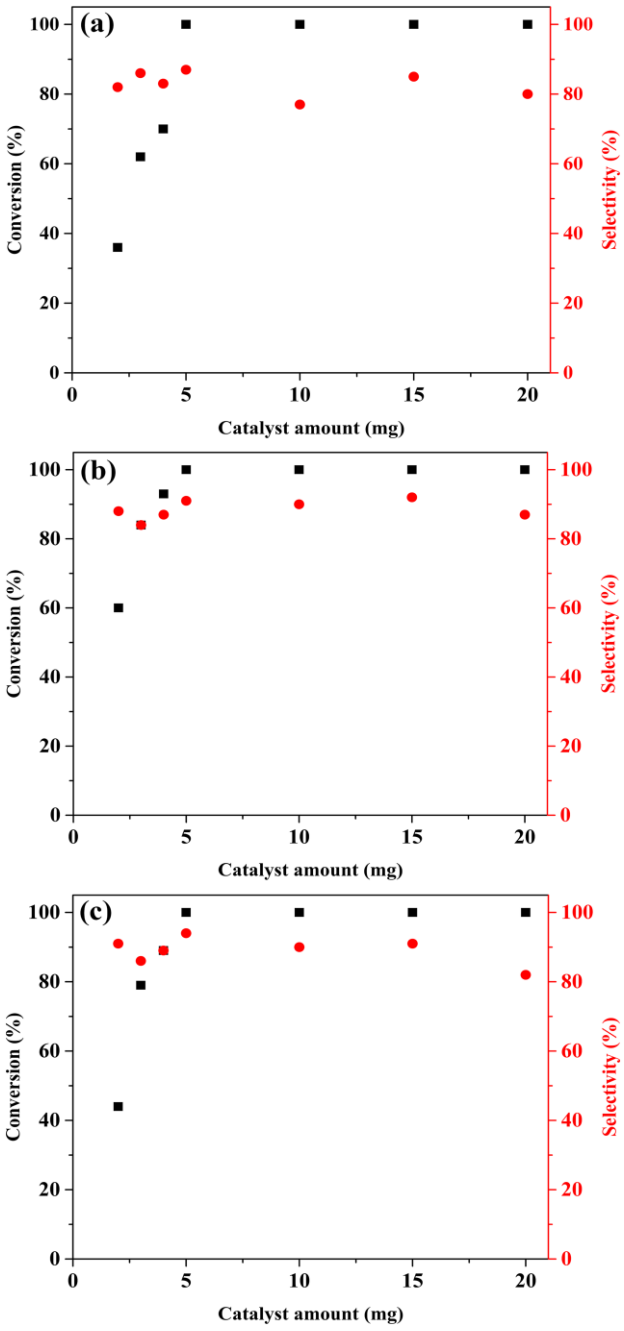

Fig. S15 The effects of catalyst amount on the oxidation of cyclohexene over (a) catalyst **1** , (b) catalyst **2** and (c) catalyst **3**. Reaction conditions; solvent: acetonitril, cyclohexene (2 mmol), TBHP (3 mmol).

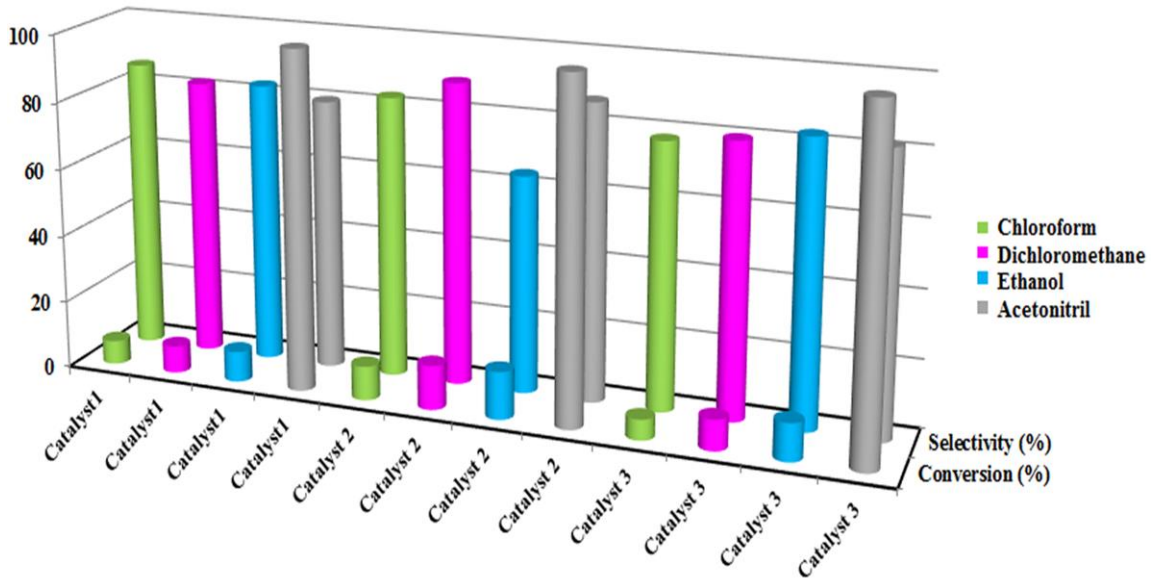

Fig. S16 The effects of solvents on the oxidation of cyclohexene by catalyst **1**, **2** and **3.**

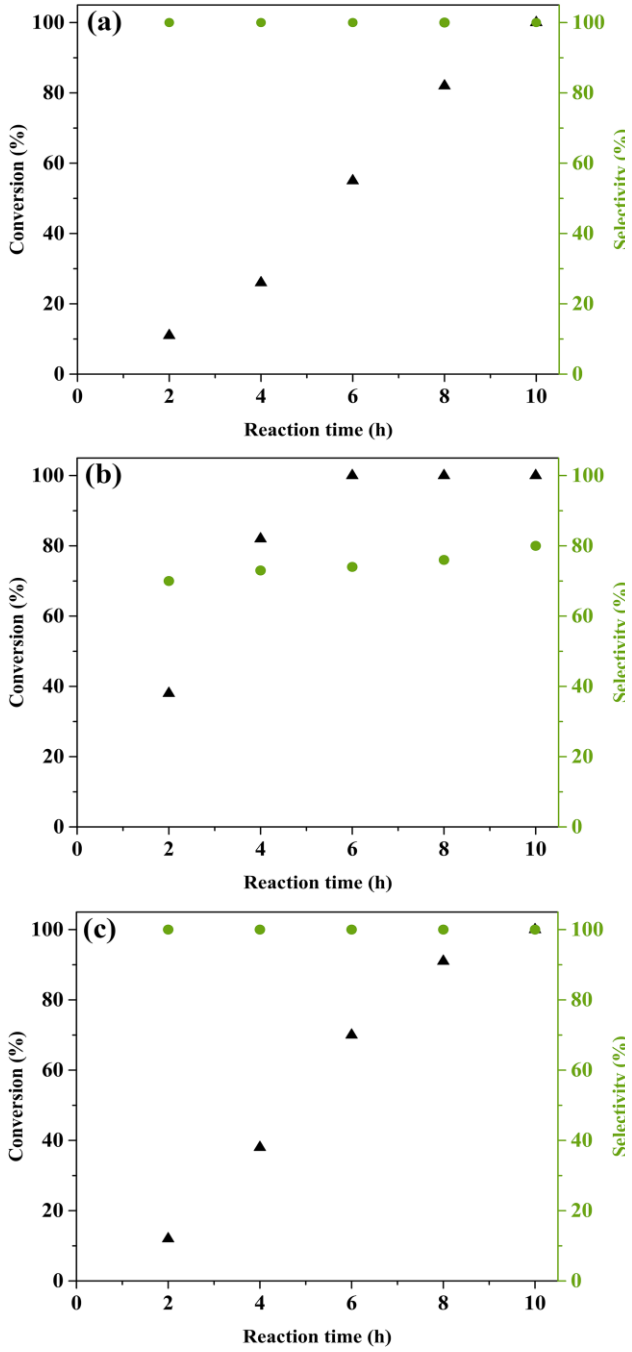

Fig. S17 Kinetic oxidation profiles of cyclooctane with TBHP over (a) catalyst **1**, (b) catalyst **2** and (c) catalyst **3**. Reaction conditions; solvent: acetonitril, cyclooctane (2 mmol), TBHP (3 mmol).

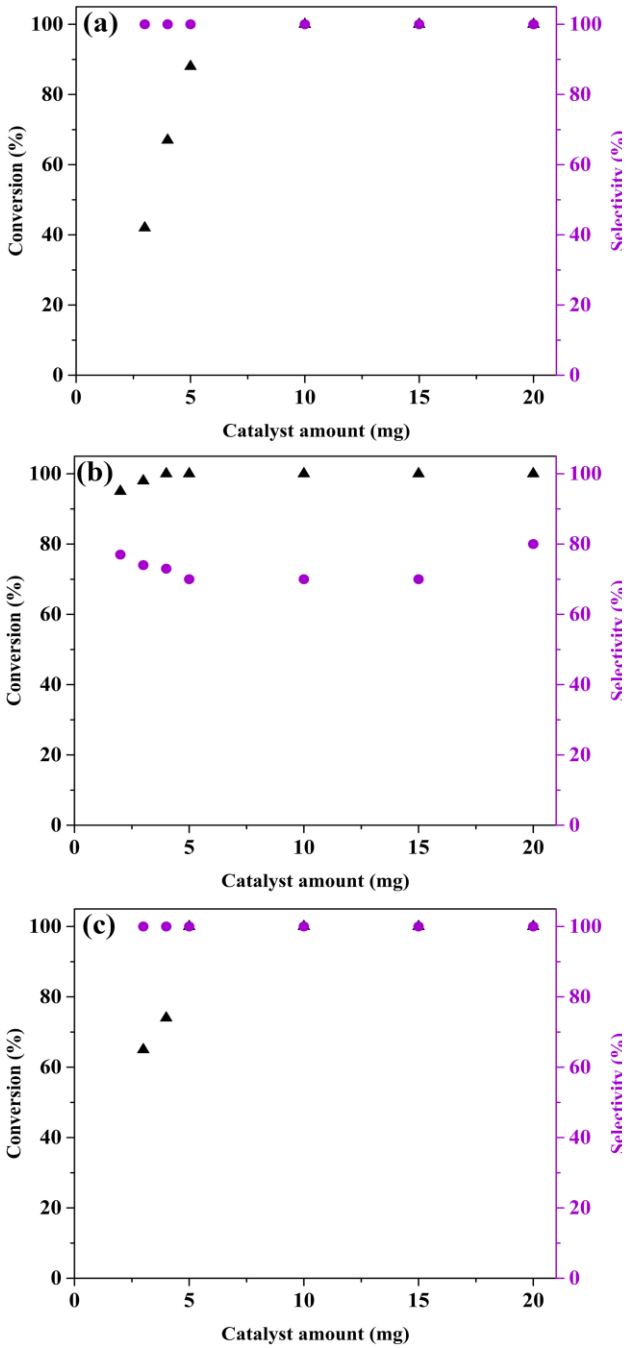

Fig. S18 The effects of catalyst amount on the oxidation of cyclooctane over (a) catalyst 1, (b) catalyst **2** and (c) catalyst **3**. Reaction conditions: solvent: acetonitril, cyclooctane (2 mmol), TBHP (3 mmol).

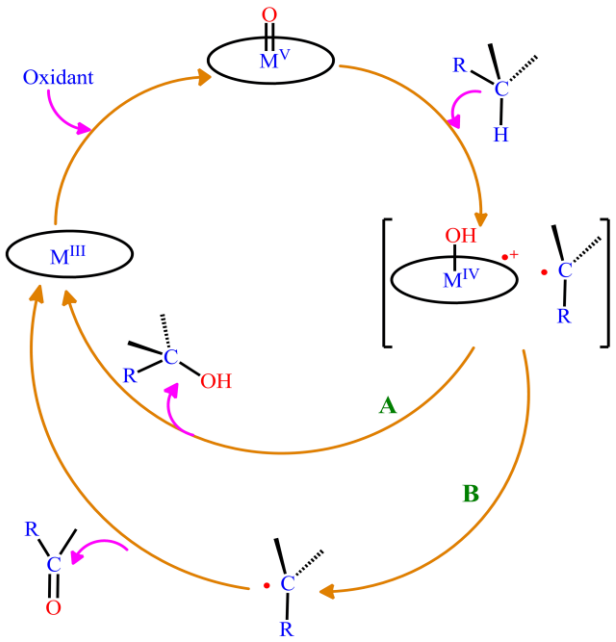

Scheme S1 Proposed mechanism for oxidation of alkanes in heterogeneous environments.

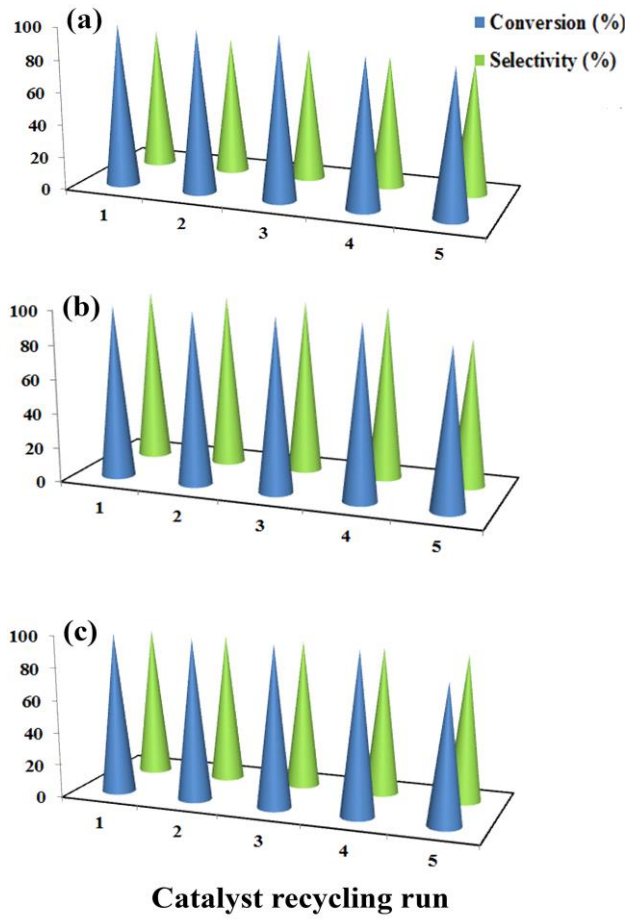

Fig. S19 The effect of recycling of (a) catalyst 1, (b) catalyst 2 and (c) catalyst 3 on epoxidation of cyclohexene.

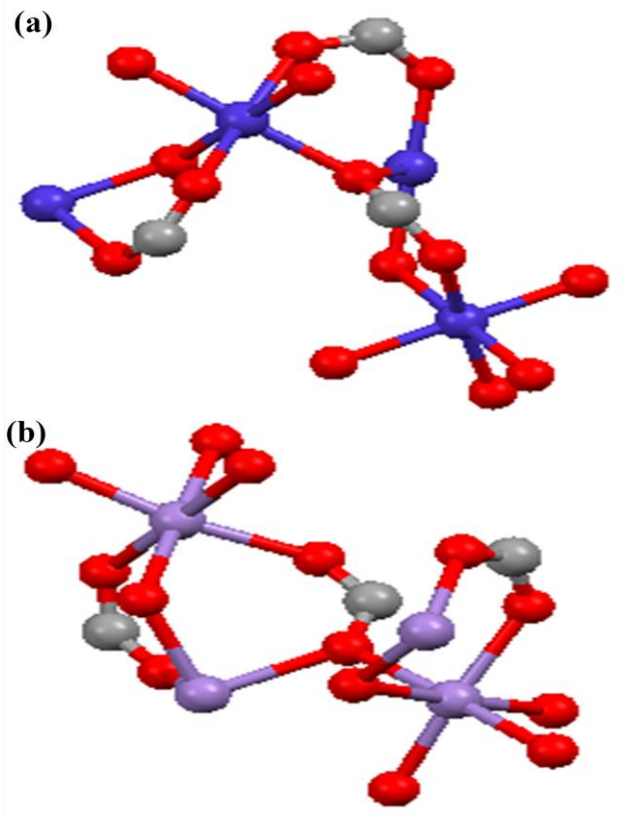

Fig. S20 The inaccessible metal sites of (a) Porph@MOM-5 and (b) Porph@MOM-6.

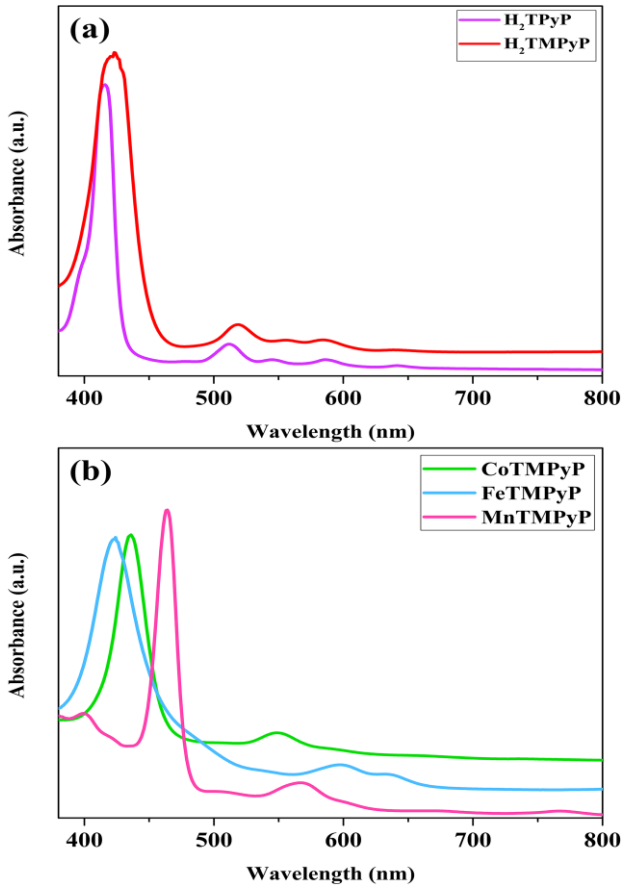

Fig. S21 UV/Vis spectra of (a) H_2TPyP (purple) in DMF and H_2TMPyP (red) in water, (b) FeTMPyP (blue), CoTMPyP (green) and MnTMPyP (pink) in water.

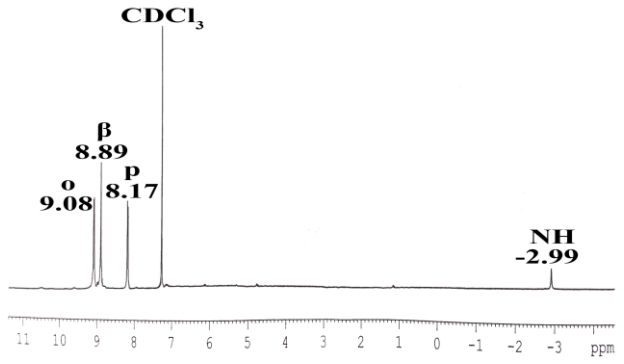

Fig. S22 ^{1}H NMR spectra of H_2TPyP.

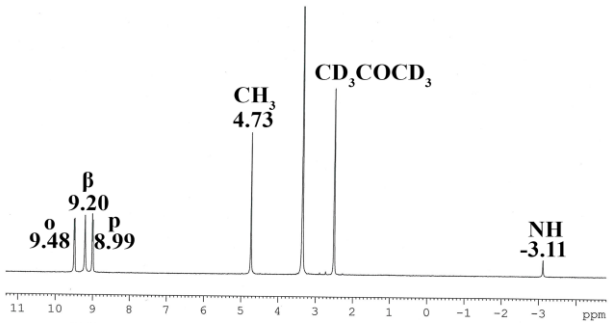

Fig. S23 ^{1}H NMR spectra of H_2TMPyP.

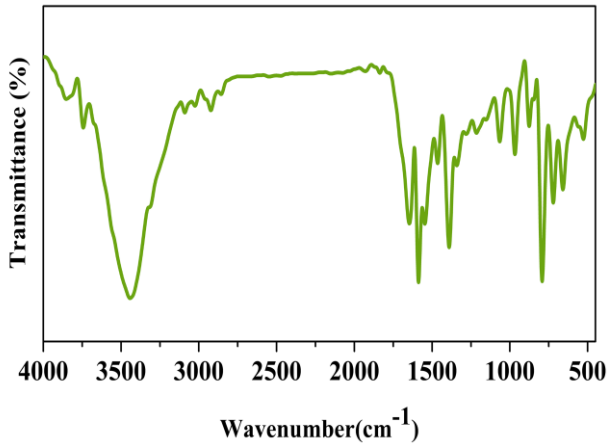

Fig. S24 FT-IR spectra of H_2TPyP.

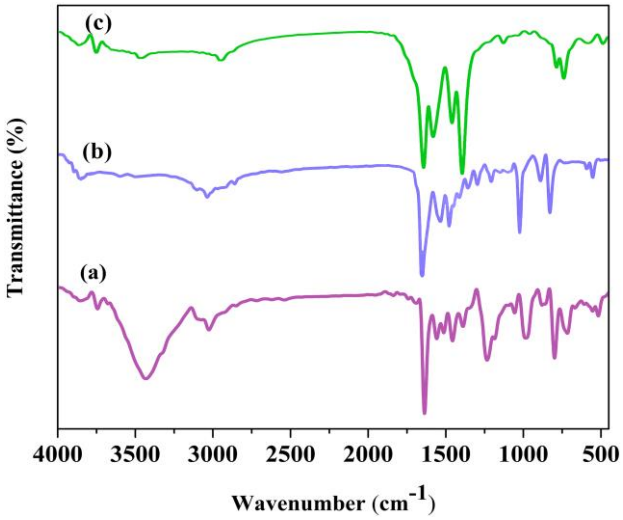

Fig. S25 FT-IR spectra of (a) H_2TMPyP, (b) CoTMPyP and (c) Porph@MOM-5.

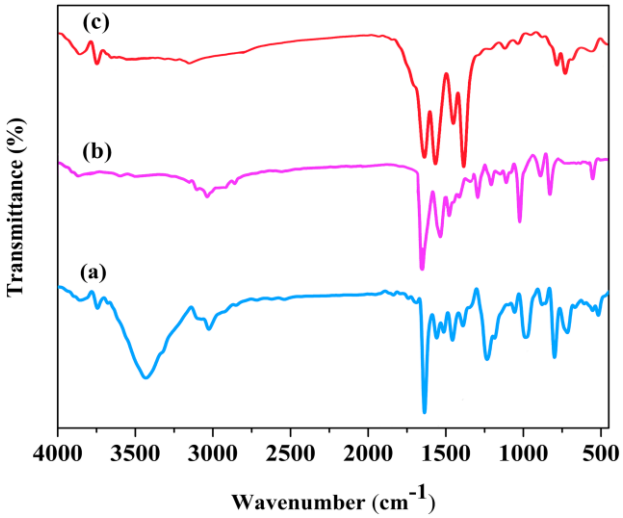

Fig. S26 FT-IR spectra of (a) H_2TMPyP, (b) MnTMPyP and (c) Porph@MOM-6.

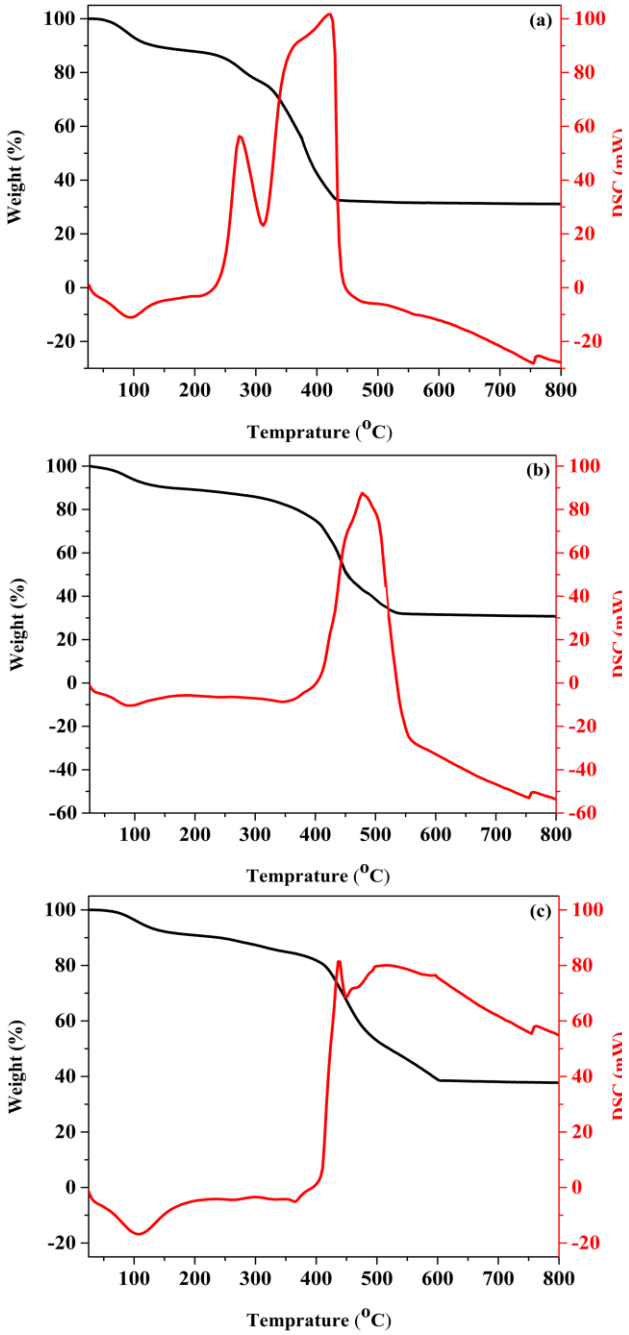

Fig. S27 TGA-DSC curves of (a) Porph@MOM-4, (b) Porph@MOM-5 and (c) Porph@MOM-6.

References

1. R. G. Little, J. A. Anton, P. A. Loach and J. A. Ibers, *Journal of Heterocyclic Chemistry*, 1975, **12**, 343-349.
2. D. Aviezer, S. Cotton, M. David, A. Segev, N. Khaselev, N. Galili, Z. Gross and A. Yayon, *Cancer Research*, 2000, **60**, 2973-2980.
3. R. F. Pasternack, H. Lee, P. Malek and C. Spencer, *Journal of Inorganic and Nuclear Chemistry*, 1977, **39**, 1865-1870.
4. R. F. Pasternack, E. G. Spiro and M. Teach, *Journal of Inorganic and Nuclear Chemistry*, 1974, **36**, 599-606.
5. A. Harriman and G. Porter, *Journal of the Chemical Society, Faraday Transactions 2: Molecular and Chemical Physics*, 1979, **75**, 1532-1542.
6. M. Sanchez-Sanchez, I. de Asua, D. Ruano and K. Diaz, *Crystal Growth & Design*, 2015, **15**, 4498-4506.
7. J. He, Y. Zhang, Q. Pan, J. Yu, H. Ding and R. Xu, *Microporous and Mesoporous Materials*, 2006, **90**, 145-152.
8. J. Chen, M. Ohba and S. Kitagawa, *Chemistry Letters*, 2006, **35**, 526-527.
9. Z. Zhang, L. Zhang, L. Wojtas, M. Eddaoudi and M. J. Zaworotko, *Journal of the American Chemical Society*, 2012, **134**, 928-933.
10. M. Gouterman, *Journal of Molecular Spectroscopy*, 1961, **6**, 138-163.
11. M. M. El-Nahass, H. M. Zeyada, M. S. Aziz and M. M. Makhlouf, *Spectrochimica Acta Part A: Molecular and Biomolecular Spectroscopy*, 2005, **61**, 3026-3031.
12. J. Qu and P. M. Fredericks, *Spectrochimica Acta Part A: Molecular and Biomolecular Spectroscopy*, 2000, **56**, 1637-1644.